EARLY AGE BEHAVIOUR OF MASSIVE CONCRETE PIERS

G. Bertagnoli*, G. Mancini* & F. Tondolo*

*Politecnico di Torino
Dipartimento di Ingegneria Strutturale e Geotecnica

Key words: concrete, early age, young hardening, cracking, thermal, massive, casting

Abstract: *In the proposed work the study of the structural effects of hydration heat and differential shrinkage on structures realized by means of massive concrete castings is presented. The object of the study are several circular piers of a viaduct built in Northern Italy.*
In the first weeks after the removal of the scaffoldings an evident crack pattern was noticed on the body of a great number of piers. The crack opening was of a few tenth of millimetres. The formation of the cracks also occurred before the dead load of the girder and the service loads were applied.
Aim of this work is the numerical simulation of what occurred to the structure in the first hours after the casting and in the following days, in order to establish the causes of the unforeseen cracking.
A diffused cracking phenomenon rising in the first days after the casting with a pattern similar to the one seen in situ has been numerically reproduced by means of a non linear finite element coupled thermal and mechanical analysis. Crack width was then calculated according to Model Code 90 and Eurocode 2 formulations, obtaining results in good agreement with the values measured in site.
The result obtained gives a clear answer of what were the main causes of the damage: hydration heat, absence of curing, dimension of the casting, differential shrinkage, evolution of concrete mechanical properties in time during the hardening reaction.

1. DESCRIPTION OF THE STRUCTURE

1.1 The Viaduct

The viaduct object of the anomalous cracking phenomenon is long several hundreds of meters and it is realized with a series of two parallel continuous girders of three spans each, with dimension (to the pier axes) 40 – 56 – 40m.
The piers are circular, with a diameter of 350cm under the extremity support, and 450cm diameter under the intermediate supports of the continuous girder. They're all grounded on direct foundations.
The ϕ 350 piers have been built with three different typologies: solid section piers, hollow section and hollow section completely filled in a second moment.
The limit dimensions for each typology are shown in the following table.

Pier Code	Description	Diameter [cm]	Body height [cm]	Foundation thickness [cm]
S65	Tallest solid ϕ 450	450	910	180
M134D	Shortest solid ϕ 450	450	750	180
C1000	Tallest solid ϕ 350	350	1000	220
C800	Shortest solid ϕ 350	350	800	220
H825	Tallest hollow ϕ 350	350-250*	300	220
H300	Shortest hollow ϕ 350	350-250*	825	220

* Outer and inner diameter of the circular crown

Table 1: Piers limit dimensions

Piers	Outer crown	Inner crown
Solid S65 & M134D	81ϕ28 on diameter ϕ 434 cm	81ϕ28 on diameter ϕ 334 cm
Solid C1000 & C800	41ϕ28 on diameter ϕ 334 cm	41ϕ28 on diameter ϕ 234 cm
Hollow H825 & H300	44ϕ25 on diameter ϕ 334 cm	44ϕ20 on diameter ϕ 254 cm

Table 2: Vertical reinforcement

Belt number	Position	Reinforcement on each crown
1	Up to 1m from foundation extrados	ϕ20/10
2	From 1 to 2m from foundation extrados	ϕ20/20
3	Intermediate zone of variable height	ϕ16/20
4	From 1 to 2m from capital intrados	ϕ20/20
5	Down to 1m from capital intrados	ϕ20/10

Table 3: Horizontal reinforcement - circular stirrups

All the piers have an axial symmetric reinforcement distribution.
Vertical reinforcement (y direction in the f.e.m. model) is disposed on two concentric circles and it is constant along the pier height.
Horizontal reinforcement, that is to say the stirrups, is arranged in a double crown (z direction in the f.e.m. model) and it is variable along the pier height: five belts with equal characteristics can be individuated along the pier body.
Minimum bar cover is 5cm. Reinforcement details are shown in tables 2 and 3.

1.2 Materials used

The mix design of the concrete used is shown in table 4.

Ingredients	**%**	**[kg/m^3]**	**Ingredients**	**%**	**[kg/m^3]**
Filler	5%	99	Gravel 22/32	15%	287
Sand 0/2	8%	149	Cement 52.5 R IV/A		330
Sand 0/8	38%	726	Super plasticizer	4.3	[l]
Fine gravel 8/12	11%	210	Water	142	[l]
Gravel 15/22	23%	439	Water/cement ratio	0.43	[-]

Table 4: Concrete mix design

According to UNI ENV 197/1 [1], cement IV/A (Puzzolan cement) is made of 65-89% of clinker and 11-35% of puzzolan and/or micro-silica and/or silica fumes.
In accordance with MC1990 [2], the values of the mechanical properties at 28 days for this concrete, are: density = 2400 kg/m^3, R_{ck} = 37 MPa, f_{ck}= 30 MPa, f_{ctm} = 2.85 MPa, E = 33550 MPa, υ = 0.2 (Poisson ratio), $\alpha = 1* 10^{-5}$ °C^{-1} (coefficient of thermal expansion).
Reinforcement bars are made of steel FeB 44 k with (according to [1]): f_{yk} = 430 MPa, f_{tk} = 540 MPa, *Es* = 200000 MPa, $\alpha = 1* 10^{-5}$ °C^{-1} (coefficient of thermal expansion).

1.3 Cracking phenomena

On a large number of the circular piers have been noticed anomalous cracking phenomena since the first days after the removal of the scaffoldings.
In situ inspections performed on the body surface of the piers reported the presence of cracks, between 0.05 and 0.30mm wide, that marked the reinforcement pattern laying beneath the surface and a thin web of smaller cracks with random direction.
At firs glance the cause of the cracks marking reinforcement layout was attributed to the thermal phenomena related to the hydration heat of the large mass of concrete of each pier. Differential shrinkage from outer surface and inner core could also worsen the initial damage. The web of thinner cracks with random directions was related to the carbonation shrinkage that affects only few micrometers from the surface.
In order to perform thermal analysis, the information about casting time, ambient temperatures at the time of casting and crack appearance were derived from working site reports and are reported in table 5.
The ambient temperature registered during the casting seem to be in good agreement also with the Italian standard UNI 10349 [3] on climate data, that gives for that geographical

zone the following average temperatures: February 3.5°C, March 8.5°C, April 13.3°C, may 17.2°C.

Pier code	Type**	Casting date	Scaffolding removal date	Cracking report date	Ambient temperature at casting [°C]	Concrete temperature at casting [°C]
21 D	S	06/05/04	07/05/04	07/05/04	14	16
22 D	S	08/04/04	10/04/04	13/05/04	n.a.	n.a.
22 P	S	06/04/04	08/04/04	13/05/04	16	18
29 D	S	15/05/04	18/05/04	19/05/04	n.a.	n.a.
29 P	S	18/05/04	20/05/04	28/05/04	20	22
36D	HR	21-24/05/04*	24/05/04	28/05/04	n.a.	n.a.
37D	HR	17-19/05/04*	19/05/04	28/05/04	20/17*	22/18*
37 P	HR	19-20/05/04*	21/05/04	28/05/04	24/25*	25/26*
38 D	HR	12-13/05/04*	14/05/04	19/05/04	16/13*	19/16*
38 P	HR	14-15/05/04*	16/05/04	19/05/04	16/16*	19/19*
39 D	HR	03-05/05/04*	05/05/04	13/05/04	11/13*	14/16*
39 P	HR	06-08/05/04*	10/05/04	13/05/04	15/16*	19/20*
55 P	S	03/02/04	05/02/04	08/02/04	4	12
63D	S	04/02/04	06/02/04	10/02/04	8	12

* Outer crown and inner filling casting data

** Pier type: S = solid, HR = hollow refilled in a second time

Table 5: Casting data derived from working site reports

2. DESCRIPTION OF THE ANALYSIS

The piers presented in table 1 have been numerically modelled with the non linear finite element code Diana (Release 9.1). Four different thermal conditions have been taken into account: casting in cold season (air temperature of 8°C and concrete temperatures at the casting of 8 and 13°C) and casting in warm season (air temperature of 17°C and concrete temperatures at the casting of 17 and 22°C).
The simulation covers a history of 40 days from the casting, because during this time the concrete hardening reaction ends its initial transitory phase and reaches an asymptotic behaviour, that is mechanical properties of concrete reach design values, meanwhile shrinkage ends its primary phase and settles on the known behaviour well documented in bibliography. In addition to that most of the cracking phenomena were registered in situ in that period.
The following physical phenomena have been taken into account in the analysis:

1. Hydration heat produced by concrete paste during the hardening phase.
2. Heat diffusion in the concrete mass.
3. Heat dispersion from the pier body to the surrounding environment.
4. Not planar imposed deformations due to the combination of thermal and shrinkage deformations.
5. Self weight action (as no girder was present on the piers in that period).

6. Non linear mechanical behaviour of concrete: linear elastic in compression, due to the low stress level, and with smeared cracking in tension.
7. Variation of mechanical properties of concrete (compressive strength, tensile strength and modulus of elasticity) during the hydration reaction.

A key parameter of the analysis is the degree of hydration reaction *r* defined as:

$$r = \frac{Q(t,r)}{Q_{\max}} \tag{1}$$

where Q_{max} [J/m^3] is the total hydration heat produced until the end of the hydration process and $Q(t,r)$ is the total hydration heat produced from the beginning of the reaction at time *t*, that can be written as follows:

$$Q(t,r) = \int_0^t q(\tau,r)d\tau \tag{2}$$

where $q(\tau,r)$ is the gradient of heat production per unit of time, that can be described decoupling time and degree of reaction as follows:

$$q(\tau,r) = q_r(r) \cdot q_T(T) \tag{3}$$

where : $q_r(r)$ is the heat power as a function of the degree of reaction

$q_T(T)$ is the heat power as a function of the temperature

and, with a further substitution:

$$q(\tau,r) = q_{\max} \cdot q_{r,norm}(r) \cdot q_T(T) \tag{4}$$

where : $q_{\max}$ is the maximum value of $q_r(r)$

$q_{r,norm}(r)$ is $q_r(r)$ normalized to 1

$$q_T(T) = \exp\left(-\frac{c_a(T,r)}{T+273}\right)$$

where: $c_a(T,r)$ is the Arrhenius constant

The fraction $q_r(r)$ depends on concrete mix design and can be derived from the data recorded in adiabatic reactions.

2.1 Hydration heat

The chemical reactions known as cement hydration are all esotermic and generally induce a volume loss. Hydration process is deeply influenced by the mix design of concrete, the cement quantity in concrete, the water/cement ratio, the ambient temperature, the cement grinding and the level at which the reaction is.

Data about cement hydration heat are given by a wide bibliography ([4], [5], [6]); in a first approximation the hydration heat varies between 250 and 450 kJ/kg of cement.

The temperature rise in adiabatic conditions has been experimentally measured for a wide range of concretes and is available in bibliography ([7] [8] [9] [10]).

As the hydration heat of the concrete used was not known in detail, two different values for the mix design presented in paragraph 1.2 were chosen in order to envelop all the possibilities in between. The total hydration heat of the cement IV/A was supposed to range between 400 and 440 kJ/kg, which means that, for the cement dosage of 330 kg/m^3 of concrete, the total heat Q_{max} are:
Q_{max} = 330 Kg/m^3 * 4.00E5 J/kg = 1.32E8 J/m^3
Q_{max} = 330 Kg/m^3 * 4.40E5 J/kg = 1.45E8 J/m^3
Once known the temperature rise in adiabatic conditions it is possible to proceed to compute the heat development as a function of the degree of reaction according to the models proposed both by Reinhardt et al. [11] and De Shutter [12] and implemented in DIANA [13], obtaining the values presented in table 6.

Time		Concrete C400		Concrete C440	
		Degree of reaction	$q_{r,norm}(r)$	Degree of reaction	$q_{r,norm}(r)$
hours	days	[-]	[-]	[-]	[-]
1.5	0.06	0.002	0.107	0.004	0.135
4.5	0.19	0.015	0.335	0.023	0.409
6.5	0.27	0.038	0.723	0.059	0.821
8.5	0.35	0.081	1.000	0.126	1.000
9.5	0.40	0.109	0.969	0.170	0.895
11.0	0.46	0.150	0.777	0.235	0.641
12.5	0.52	0.187	0.561	0.292	0.420
15.0	0.63	0.233	0.338	0.365	0.226
18.5	0.77	0.278	0.181	0.434	0.109
24.0	1.00	0.320	0.112	0.500	0.047
48.0	2	0.438	0.040	0.602	0.013
72.0	3	0.522	0.024	0.661	0.010
96.0	4	0.582	0.014	0.704	0.008
144.0	6	0.666	0.007	0.763	0.005
384.0	16	0.870	0.004	0.908	0.004
720.0	30	1.000	0.000	1.000	0.000

Table 6: Hydration heat description for the selected concretes

2.2 Specific heat

The specific heat or thermal capacity per unit volume of concrete [J/(m^3 °K)] is a function of the density, the water/cement ratio, the degree of hydration, the temperature of the paste. For medium density structural concretes Neville [14] gives the value of = 2.02E6 J/(m^3 °K). Other values or specific formulations were proposed by Waller [15], Mandry [16], Ballim [17], the ACI [18], the JCI [19] and the ICOLD [20]. De Schutter [21] also gives a formulation for the variation of the specific heat with the degree of reaction.

For the present study the thermal capacity of both the foundation and the pier body is set constant and equal to 840 J/(kg °C), that is to say 2.02E6 J/(m^3 °C).

2.3 Thermal conductivity

Thermal conductivity is the heat quantity transmitted through a unit surface to a unit distance in a unit of time under a unit thermal gradient [J/(s m^2 °K/m)]. Its value is influenced by the same factors that modify the specific heat seen in the former paragraph. For standard concretes at complete hydration many values of this physical property can be found in bibliography (Neville [14], the ACI [18], the JCI [19], the ICOLD [20], UNI 7357 [22], Hund [23]). De Schutter [21] also gives a formulation for the variation of the thermal conductivity with the degree of reaction.
For the present study the thermal conductivity of the pier body is linearly variable with the degree of reaction *r* between 2200 J/(s m^2 °K/m) for *r=0*, and 1000 J/(s m^2 °K/m) for *r=1*, while the value for *r=1* is also applied to the foundation.

2.4 Heat dispersion in the surrounding environment

The heat transfer between solid bodies, i.e. the pier or the foundation, and the atmosphere takes place involving the three phenomena of conduction, convection and irradiation.
The superposition of these three channels of heat exchange, among which convection plays the most important role, is conventionally simplified by means of an equivalent thermal conductivity K_e [J/(s m^2 °K)], whose values depends on environmental conditions.
For instance the Italian standard UNI 7357-74 [22] gives the following data for open air conditions and wind up to 4m/s:

Horizontal surface, upward heat flow	$K_e = 20$
Vertical surface, parallel heat flow	$K_e = 20$
Horizontal surface, downward heat flow	$K_e = 14$

For stronger wind conditions these values can be corrected with a proposed formulation.
Similar values and correlations with wind speed are given by Sikoku [24], the ICOLD [20] and the JCI [19]. For the present study the equivalent thermal conductivity with respect to the atmosphere is settled constant and equal to 20 J/(s m^2 °K).
A similar phenomenon occurs at the interface between the foundation and the soil: an equivalent thermal conductivity of 2 J/(s m^2 °K) has been adopted in this case.

2.5 Mechanical properties variation during hydration

Mechanical properties of concrete deeply change during the hydration process as the material changes from fluid to solid state. In the computational model concrete is always seen as a solid material, whose mechanical properties are very low at the beginning of the hydration reaction and rise while the reaction takes place.
In this study the variation of compressive strength, tensile strength and modulus of elasticity, has been taken into account in accordance with MC90 [2], Carino [25] , Breguel [26] and De Shutter [27].
The Model Code 90 limits the application of the proposed formula to the starting age of 3 days for concrete, when the mechanical properties are approximately ranging between $^1/_3$ and ½ of their values at 28 days. Moreover the formulations proposed are calibrated for

isothermal curing at 20°C according to ISO 2736/2 and no clue is given for tensile strength variation.
Carino [25] proposes a formulation that relates the development of compressive resistance in time, since 1 day after casting, to different isothermal curing temperatures ranging from 5°C to 43°C. Breguel [25] and de Shutter [26] relate the development of compressive strength, tensile strength and modulus of elasticity to the degree of reaction *r* for concretes made with CEM I, CEM IIIB and CEM IIIC.
Grounding on the formulations proposed ([25] & [26]), specific functions for the evolution of material properties have been developed for our mix design and have been calibrated on laboratory test performed on cubic specimens and summarized in table 7.

	Laboratory test					Working site test
Specimens age [Days]	$R_{c,min}$ [MPa]	$R_{c,min}$ adim. [-]	$R_{c,max}$ [MPa]	$R_{c,max}$ adim. [-]	R_{cm} [MPa]	R_{cm} [MPa]
2	20.6	0.52	22.3	0.53	21.5	19.0
7	30.2	0.76	33.0	0.78	31.5	32.6
14	37.9	0.95	39.5	0.94	38.8	37.4
28	39.9	1.00	42.2	1.00	41.4	41.4

Table 7: compressive strength test on cubic specimens

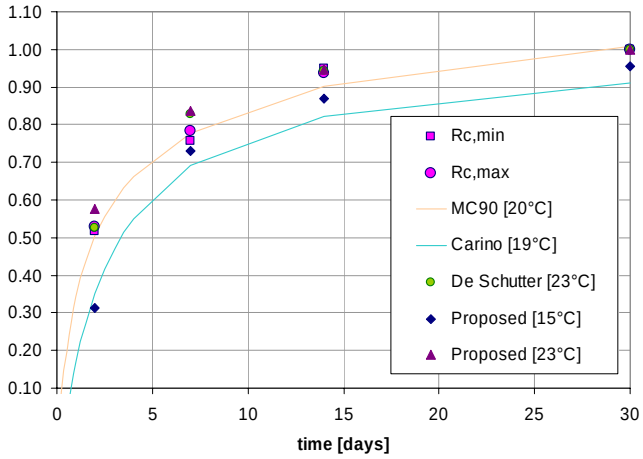

Figure 1: Compression strengths in isothermal curing

Two cubic specimens have been numerically modelled with isothermal curing at constant temperatures of 15°C and 23°C, to envelop the real curing conditions that lead to the minimum and maximum values registered in laboratory.

The results of real specimens, Model Code 90 proposal for 20°C isothermal curing, Carino proposal for 19° isothermal curing, De Shutter values for CEM I (Portland cement 52.5), that is the most similar to the one used for the piers, have been compared in figure 1.

2.6 Shrinkage

Shrinkage has been modelled according to MC90 [2]. As drying shrinkage is sensibly influenced by the hydraulic radius of the member, it's reasonable to suppose that it has been greater in the regions of the pier near the outer surface than in the inner core.
The piers body has then been divided into 4 cylindrical concentric crowns for which a different shrinkage function has been calculated. The four zones have the following thicknesses: the first one from the surface to 25cm of depth, the second one from 25cm to 50cm of depth, the third one from 25cm to 50cm of depth and the fourth and last one from 100cm of depth to the axis of the pier.
These dimension have been chosen in order to have a smooth variation of shrinkage from one zone to the other; different thicknesses in a range of ± 20% don't lead to results sensibly different from the ones proposed.
An example of the shrinkage curves obtained is shown in figure 2.

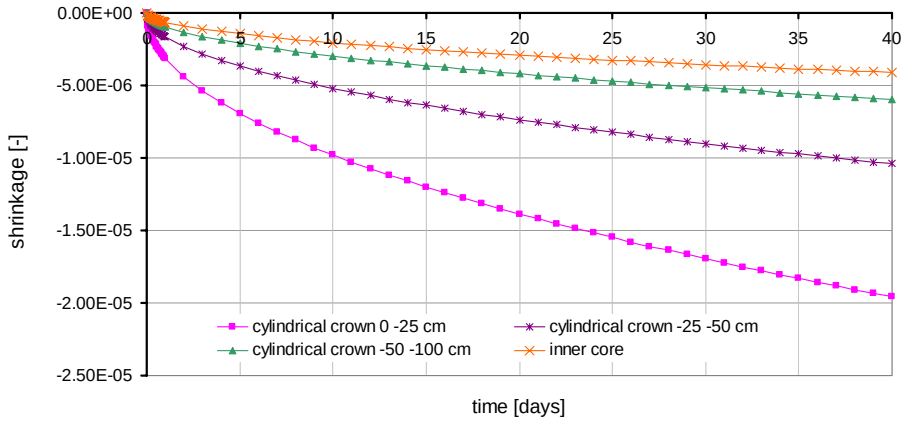

Figure 2: Shrinkage values for ϕ450 piers

2.7 Mesh description

The pier body is characterized by axial symmetry both for the concrete geometry and for the reinforcement layout. All the actions taken into account and summarized before benefit also of the axial symmetry. It was then possible to solve the problem with a plane model in axial symmetry. The meshes used for the four solid body piers are shown in figure 3: concrete elements (8 nodes) are drawn in pink, while reinforcement layers are in blue.
The modelling of hollow core pier with subsequent filling required a better refined mesh and a phased analysis. In a first phase lasting 24h, only the external 50cm thick circular

crown and the foundation were present. In the second phase, lasting from day 1 to 40, the inner core elements were introduced and the coupled behaviour was analyzed.
The foundations were modelled mostly because of thermal diffusion reasons and to simulate the restraint at the base of the pier. Such structures, common to each couple of piers that bears the parallel girders, are not axial symmetric in reality. The modelling of the whole foundation is almost useless, as all the phenomena taken into account decrease their intensity while increasing the distance from the pier. It was then modelled a cylindrical portion of the foundation with radius 1m greater than the pier one and with the real thickness of the foundation (180 cm for ϕ450 and 220cm for ϕ350).
Even if cast with the same concrete of the pier bodies, the foundations had an age of few months when the upper casting took place. Their residual hydration process and shrinkage were therefore neglected in the analysis.

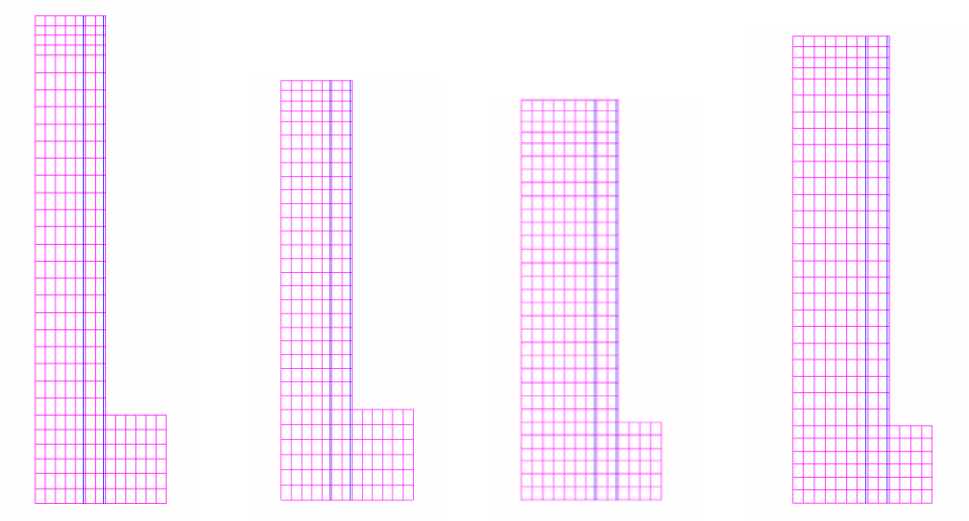

C1000	C800	M134D	S65
ϕ350 h=10.0m	ϕ350 h=8.0m	ϕ450 h=7.5m	ϕ450 h=9.1m

Figure 3: Solid body piers meshes

3. F.E.M. ANALYSIS RESULTS

The f.e.m. analysis allowed the evaluation in time of temperature and stresses variation, both in concrete and in steel. The crack patterns for different load cases have been also evaluated.
The extreme values of the temperatures and the stresses reached during the analysis in each pier in different conditions are presented in table 8.
Each pier is identified by a code, that is represented by a string where it is possible to read in sequence: the name of the pier (see table 1), the type of cement used (400 or 440 kJ/kg), concrete temperature at casting (8-13-17-22°C), ambient temperature at casting (8-17°C).

Pier code	Max. inner tempe-rature [°C]	Max. surface tempe-rature [°C]	Vertical Bars Max. stress [MPa]	Stirrups Max. stress [MPa]	Vertical Bars Stress at 40 days [MPa]	Stirrups Stress at 40 days [MPa]
S65_400_8_8	46	22	66	44	10	5 ÷ 10
S65_400_13_8	52	25	130	51	0 ÷ 20	5 ÷ 10
S65_400_17_17	56	34	140	47	0 ÷ 20	5 ÷ 10
S65_400_22_17	61	37	158	54	5 ÷ 20	5 ÷ 10
S65_440_8_8	58	26	106	57	0 ÷ 25	5 ÷ 15
S65_440_13_8	61	29	172	65	0 ÷ 20	5 ÷ 15
S65_440_17_17	65	39	183	60	0 ÷ 35	5 ÷ 15
S65_440_22_17	70	43	187	68	0 ÷ 20	5 ÷ 15
134D _400_8_8	46	22	51	44	0 ÷ 10	0 ÷ 10
134D _400_13_8	52	25	120	51	0 ÷ 30	0 ÷ 10
134D _400_17_17	56	34	52	47	0 ÷ 10	0 ÷ 10
134D _400_22_17	61	37	61	54	0 ÷ 10	0 ÷ 10
134D_440_8_8	58	26	80	57	0 ÷ 20	0 ÷ 15
134D _440_13_8	61	29	84	65	0 ÷ 20	0 ÷ 15
134D _440_17_17	65	39	64	60	0 ÷ 10	0 ÷ 15
134D _440_22_17	70	43	157	68	0 ÷ 40	0 ÷ 15
C1000 _400_8_8	43	21	47	36	0 ÷ 5	0 ÷ 5
C1000 _400_13_8	48	24	61	42	0 ÷ 5	0 ÷ 5
C1000 _400_17_17	54	34	63	41	0 ÷ 5	0 ÷ 5
C1000 _400_22_17	59	37	84	47	0 ÷ 5	0 ÷ 5
C1000_440_8_8	52	25	103	46	0 ÷ 5	0 ÷ 5
C1000 _440_13_8	58	28	150	54	0 ÷ 5	0 ÷ 5
C1000 _440_17_17	63	38	120	53	0 ÷ 5	0 ÷ 5
C1000 _440_22_17	58	42	135	59	0 ÷ 5	0 ÷ 5
C800 _400_8_8	43	21	47	35	0 ÷ 5	0 ÷ 5
C800 _400_13_8	48	24	63	42	-5 ÷ 5	-5 ÷ 5
C800 _400_17_17	54	34	57	41	-5 ÷ 5	-5 ÷ 5
C800 _400_22_17	59	37	64	47	-5 ÷ 5	-5 ÷ 5
C800_440_8_8	52	25	67	46	-5 ÷ 5	-5 ÷ 5
C800 _440_13_8	58	28	85	54	-5 ÷ 5	-5 ÷ 5
C800 _440_17_17	63	38	78	53	-5 ÷ 5	-5 ÷ 5
C800 _440_22_17	68	42	135	61	-5 ÷ 5	-5 ÷ 5
HR_300_400_8_8	41	15	48	33	-5 ÷ 5	-5 ÷ 5
HR_800_400_8_8	42	15	67	36	0	0
HR_300_440_22_17	36	34	-10÷+12	-17÷-10	-5 ÷ 0	-10 ÷ 0
HR_825_440_22_17	34	32	-17÷+5	-15 ÷ 5	-7 ÷ 0	-10 ÷ 0

Table 8: Extreme temperature and stresses reached in the analysis

4. CRACK WIDTH CALCULATION

This paragraph presents the calculation of the crack width in the most damaged zones of each pier analyzed by f.e.m.. Such calculation is made according to the indications provided in MC90 [2] and ENV 1992-1-1 [3]. The results obtained with the two methods are quite similar, nevertheless it's useful to highlight some considerations before presenting the results:

1. Bibliography lacks a consolidated formulation intended to calculate crack width in the first week after the casting, that is when mechanical properties of concrete are quickly changing in time. The models proposed by MC90 and ENV 1992-1-1 [3] have been calibrated for calculating crack width in times far from the casting and with material strengths close to 28 days values.
2. The finite element model used implements a "smeared" crack approach. The position and amplitude of the single cracks are not direct results of the numerical analysis but had to be extrapolated by the use of empirical or experimental models suggested by normative codes.

The geometrical input data for the calculation of horizontal and vertical cracks respectively are resumed in table 9 and 10.

d' = distance between vertical bar axis and external surface	80	[mm]
t = 2.5d' thickness of the concrete external circular crown controlled by reinforcement	200	[mm]
ϕ28 bars in the external crown of piers ϕ450	80	[-]
ϕ28 bars in the external crown of piers ϕ350 (solid body)	41	[-]
ϕ25 bars in the external crown of piers ϕ350 (hollow core)	44	[-]
Area of the circular crown (piers ϕ450)	2700400	[mm^2]
Area of the circular crown (piers ϕ350)	2072400	[mm^2]
geometrical reinforcement ratio (piers ϕ450)	0.018	[-]
geometrical reinforcement ratio (piers ϕ350 solid body)	0.012	[-]
geometrical reinforcement ratio (piers ϕ350 hollow core)	0.010	[-]

Table 9: Geometrical input data for horizontal cracks

d' = distance between vertical bar axis and external surface	60	[mm]
t=2.5d' thickness of the concrete external circular crown controlled by reinforcement	150	[mm]
geometrical reinforcement ratio (ϕ 20/10)	0.021	[-]
geometrical reinforcement ratio (ϕ 20/20)	0.010	[-]
geometrical reinforcement ratio (ϕ 16/20)	0.007	[-]

Table 10: Geometrical input data for vertical cracks

The distances between cracks have been calculated according to MC90 (equation 5) and ENV 1992-1-1 (equation 6). The results are presented in table 11.

$$l_{s,\max} = \frac{\phi_s}{3.6\rho_{s,ef}} \tag{5}$$

$$l_{s,\max} = 50 + 0.25k_1 \cdot k_2 \cdot \phi / \rho_{s,ef} \tag{6}$$

Distances between cracks [cm]	MC 90	ENV 1991-1-1
Distance between horizontal cracks (piers ϕ450)	43	36
Distance between horizontal cracks (piers ϕ350 solid body)	64	51
Distance between horizontal cracks (piers ϕ350 hollow core)	67	63
Distance between vertical cracks (ϕ20/10 belt)	27	31
Distance between vertical cracks (ϕ20/20 belt)	53	56
Distance between vertical cracks (ϕ16/20 belt)	66	69

Table 11: Distance between cracks

Cracks width was calculated according to MC90 (equation 7) and ENV 1992-1-1 (equation 8).

$$w_k = l_{s,\max}\left(\varepsilon_{sm} - \varepsilon_{cm}\right) \tag{7}$$

$$w_k = \beta \cdot l_{s,\max} \cdot \varepsilon_{sm} \tag{8}$$

The results are presented in table 12 and 13 using the following symbols:

t_{beg}	time of first cracking (in hours)	ε_{sr2}	steel strain at first cracking
ε_c	total strain in concrete	$t_{\max}$	time of maximum crack width
$\varepsilon_{c\Delta T}$	thermal strain in concrete	ε_{s2}	steel strain in bare bar condition

Pier code	At first cracking				At max crack width			
	t_{beg}	ε_c	$\varepsilon_{c\Delta T}$	ε_{sr2}	$t_{\max}$	ε_{s2}	w_m	
							MC90	EN1992
	[h]	[-]	[-]	[-]	[h]	[-]	[mm]	[mm]
S65_440_22_17	20	7.50E-05	3.40E-05	4.10E-05	72	8.9.E-04	0.37	0.32
134D _440_22_17	18	6.70E-05	2.38E-05	4.32E-05	111	7.5.E-04	0.31	0.27
1000 _440_22_17	20	8.45E-05	3.59E-05	4.86E-05	70	6.4.E-04	0.39	0.33
800 _440_22_17	20	8.40E-05	3.62E-05	4.78E-05	97	4.4.E-04	0.39	0.33
HR_300_400_8_8	84	5.75E-05	4.00E-05	1.75E-05	140	2.3.E-04	0.14	0.12
HR_825_400_8_9	84	4.40E-05	3.60E-05	8.00E-06	195	3.2.E-04	0.20	0.16

Table 12: Horizontal crack width

Pier code	At first cracking				At max crack width			
	t_{beg}	ε_c	$\varepsilon_{c\Delta T}$	ε_{sr2}	$t_{\max}$	ε_{s2}	w_m	
							MC90	EN1992
	[h]	[-]	[-]	[-]	[h]	[-]	[mm]	[mm]
S65_440_22_17	18	5.70E-05	2.18E-05	3.52E-05	83	3.2.E-04	0.20	0.22
134D _440_22_17	16	5.68E-05	1.24E-05	4.44E-05	54	3.2.E-04	0.20	0.22
1000 _440_22_17	16	7.78E-05	2.26E-05	5.52E-05	70	2.8.E-04	0.16	0.19
800 _440_22_17	16	1.00E-04	1.23E-05	8.77E-05	40	2.9.E-04	0.16	0.18
HR_300_400_8_8	90	6.40E-05	4.00E-05	2.40E-05	140	1.6.E-04	0.09	0.11
HR_825_400_8_9	90	5.50E-05	4.30E-05	1.20E-05	150	1.7.E-04	0.11	0.12

Table 13: Vertical crack width

We are then lead to the following conclusions:

1. The maximum width of horizontal cracks varies between 0.15 e 0.40mm.
2. Such value is reached at the peak of the phenomenon, that is to say between 2 and 3 days from the casting, and tends to reduce during the first month.
3. This process that leads the cracks to re-closing is hindered by negative friction due to aggregate interlock: a prediction of cracks width in long time is then difficult.
4. Vertical cracks have a theoretical distance similar to horizontal ones (more or less 50 cm against 54 cm), but a smaller width (0.10-0.25mm).
5. A number of piers result to have only four vertical macro-cracks located approximately at the four quadrants of the circular section. If we force this distance in our model we obtain crack widths of the order of 0.60-1.20mm, which were commonly found on the real structures.

5. CONCLUSIONS

The results of the analysis described in the paragraphs above can be synthesized as follows:

1. All the solid body piers and the hollow core ones filled in a second time are interested by cracking in the external cortex layer. Hollow core piers not filled in a second time present very little or no cracking at all in the first 40 days of life.
2. Cracks interest the full height of the pier body in the first 5 days after the casting.
3. The depth of the cracked region is different in each pier and varies in time. In the worst cases it reaches the second layer of reinforcement (50cm approximately from the surface), but the crack width tends to reduce itself with time.
4. The cracking phenomenon reaches its apex when the mechanical properties of concrete are not fully developed.
5. The main cause of the crack formation is the thermal gradient (varying from 20 to 30°C) between the hot core of the pier and the warmer external surface.
6. The maximum temperature reached in the core of the pier subjected to the worst conditions is approximately 70°C.
7. Differential shrinkage between the inner core, better insulated, and the external surface, subjected to quicker exsiccation, enhances the negative thermal effects.

8. Piers ϕ350 had a better heat dispersion, as are leaner, so they were subjected to weaker thermal actions. Nevertheless they suffered from cracking of the same magnitude of piers ϕ450, as they are less reinforced.
9. The variations in the ambient temperature seem to play a marginal role.
10. The choice of asking high material strengths at few days after the casting achieved through a fine grinding of the cement paste (52.5) implied a quicker hydration and worsen the piers damage.
11. The stresses in reinforcement bars, both vertical and horizontal, reached values rating from 45 MPa to 190 MPa at a few days after the casting, but they fall down to values below 40 MPa at the end of the first month.
12. Concrete mix design is a key parameter: using cement named C440 we get a great number of wider cracks in a shorter time than using concrete named C400.
13. As a consequence of point 12, the cases presented in this paper were also re-run using a concrete realized with cement IIIB, with one of the lowest hydration heat available (268 kJ/kg). Even with this choice the piers were subjected to cracking, although of lesser magnitude. Then the problem can not be overcome simply by changing the mix design, being deeply related to the dimension of the casting. Possible solutions to avoid or limit cracking could be: realizing hollow core piers instead of solid body ones; casting solid body piers in several different layers in different days; using a cooling pipes system inside the body of the structure.
14. The whole phenomenon tends to exhaust in the first month of life of the structures. At this period the inner temperature drops to environmental level, the stresses both in concrete and steel are approximately turned back to zero and even the cracks tend to settle to constant width values below their peak level or to close.
15. Daily temperature cycles between day and night and further shrinkage could enhance cracks width in the following months.

REFERENCES

[1] UNI ENV 197/1
[2] CEB Bulletin d'Information n° 213/214, CEB-FIP Model Code 1990, May 1993, Thomas Thelford ed., ISBN 0 7277 1696 4
[3] UNI 10349 Dati Climatici 1974
[4] Collepardi, Mario – Scienza e tecnologia del calcestruzzo – 3° edizione – Hoepli – 1991 – ISBN 88-203-1910-1)
[5] Collepardi Mario – Il nuovo calcestruzzo – 3° edizione – Enco edizioni – 2003 – ISBN 88-203-1910-1
[6] Vito Alunno Rossetti – Il calcestruzzo, materiali e tecnologia – 2° edizione – McGraw-Hill – 2003 – ISBN 88-386-6085-9
[7] Watanabe N., Yamada K., Relation between the thermal crack and the dimension of mass concrete made of regulated set cement. International conference on concrete at early ages, Paris 6-8 april 1982.
[8] Jin Keun Kim, Kook Han Kim, Joo Kyoung Yang, Thermal analysis of hydration heat in concrete structures with pipe cooling system, Computer and Structures 79, 2001, pp. 163-171

[9] Bentz D.P., Waller V., de Larrard F., Prediction of adiabatic temperature rise in conventional and high performance concretes using a 3-D microstructural model, Cement and Concrete Research, 28, 1998, pp 285-297
[10] De Shutter G., Taerwe L., General Hydratation model for portland cement and blast furnace slag cement, Cement and Concrete Research, 25, 1995, pp 593-604
[11] Reinhardt H. W., Blaauwendraad J., Jongendijk J., Temperature development in concrete structures taking account of state dependent properties, International conference on concrete at early ages, Volume ,1 Avril 1982, Editions Anciens ENPC, ISBN 2-85978-038-6, pp 211-218.
[12] De Shutter G., Hydratation and temperature development of concrete made with blast furnace slag cement, Cement and Concrete Research, 29, 1999, pp 143-149
[13] Diana 8.1 User's Manual – Material Library – 2nd Edition May 2003
[14] A. M. Neville, Properties of concrete – Fourth and final edition, Longman ed. 1995 ISBN 0-582-23070-5
[15] Waller V, de Larrard F, Roussel P. Modelling the temperature rise in massive HPC structures. In: Utilization of high strength-high performance concrete. International Symposium, vol. 4, Paris,1996. p. 415-21.
[16] Mandry W. Uber das Kulen von Beton. Springer Verlag, Berlin 1961.
[17] Y. Ballim, P.C. Graham, Early-age heat evolution of clinker cements in relation to microstructure and composition: implications for temperature development in large concrete elements, Cement & Concrete Composites 26 (2004) 417–426
[18] ACI Committee 207, Mass Concrete. ACI Manual of Concrete Practice, Part 1, 207.1, 1994. p. 21±3.
[19] JCI Committee on the thermal stress. The state of the art report of thermal stress evaluation in massive concrete, 1985. p. 5±9.
[20] Commission Internationale des Gran Barrages (ICOLD), Thermal analysis of a RCC Dam Body During Construction, 7th Benchmark Workshop on Numerical Analysis of Dams September 24-26 2003 Bucharest Romania.
[21] De Schutter G., Finite element simulation of thermal cracking in massive hardening concrete elements using degree of hydratation based materials laws, Computer and structures 80, 2002, pp. 2035-2042.
[22] UNI 7357-74 Calcolo del fabbisogno termico per il riscaldamento degli edifici 1974
[23] Hund J. Wagner A. „Einfluss des Feuchtigkeitsgehaltes und des Reifegrades auf die Warmeileitfahigkeit von Beton". Deutscher Ausschuss fur stahlbeton, H.297, Verlag Emst & Sohn, Berlin 1978
[24] Sikoku Electric Power Corp., A study on the preventive measure of early age cracking in a mass concrete. Technical report, 1964.
[25] Carino N.J., Maturity functions for concrete, International conference on concrete at early ages, Volume 1, Avril 1982, Editions Anciens ENPC, ISBN 2-85978-038-6, pp 123-128
[26] Breguel K. Van, Developement of temperature and properties of concrete as a function of the degree of Hydratation, International conference on concrete at early ages, Volume 1, Avril 1982, Editions Anciens ENPC, ISBN 2-85978-038-6, pp 179-185
[27] De Shutter G., Taerwe L., Degree of hydratation based description of mechanical properties of early age concrete, Materials and Structures, 29, 1996, pp.335-344